NASA TECHNICAL NOTE

NASA TN D-3708

NASA TN D-3708

EXPERIMENTAL INVESTIGATION OF TRANSVERSE-MODE SOLID-PROPELLANT COMBUSTION INSTABILITY IN A VORTEX BURNER

by Louis A. Povinelli, Marcus F. Heidmann, and Charles E. Feiler

Lewis Research Center
Cleveland, Ohio

NATIONAL AERONAUTICS AND SPACE ADMINISTRATION • WASHINGTON, D. C. • NOVEMBER 1966

NASA TN D-3708

EXPERIMENTAL INVESTIGATION OF TRANSVERSE-MODE SOLID-PROPELLANT COMBUSTION INSTABILITY IN A VORTEX BURNER

By Louis A. Povinelli, Marcus F. Heidmann, and Charles E. Feiler

Lewis Research Center
Cleveland, Ohio

NATIONAL AERONAUTICS AND SPACE ADMINISTRATION

For sale by the Clearinghouse for Federal Scientific and Technical Information
Springfield, Virginia 22151 – Price $2.00

EXPERIMENTAL INVESTIGATION OF TRANSVERSE-MODE SOLID-PROPELLANT COMBUSTION INSTABILITY IN A VORTEX BURNER

by Louis A. Povinelli, Marcus F. Heidmann, and Charles E. Feiler

Lewis Research Center

SUMMARY

Transverse mode combustion instability was investigated by using a two-dimensional vortex or pancake-type combustor in which the oscillations were cause by a swirling tangential flow supplied by a progressively burning gas generator. The pressure level, pressure amplitude, and frequency of oscillation were measured for various propellant compositions and motor nozzle diameters. Fundamental changes in the propellant flame behavior were made by changing the oxidizer particle size and the pressure. The data were interpreted in terms of a calculated response function based on the Rayleigh criterion for wave amplification. Use of radially drilled rings was effective in eliminating instability. The damping effect was consistent with the postulated driving mechanism.

INTRODUCTION

A certain degree of experimental success has been achieved in understanding the interaction between the flow field and the combustion processes in solid-propellant rocket motors. Similarly, theoretical analyses have been successful in predicting the intermittent instability behavior similar to that occurring during rocket-motor firings. It is evident, however, that the current understanding of combustion stability, although helpful, is such that a prediction of the unsteady burning behavior of rocket motors is not always possible. Evidence of tangential flow in full-scale engines exists; for instance, the third stage of the Scout ST-1 vehicle was believed to oscillate in the tangential mode accompanied by a roll disturbance (ref. 1). This disturbance appears to result from a nonlinear viscous phenomenon (acoustic streaming) which occurs in the presence of large amplitude acoustic wave motion (refs. 2 and 3). For the Scout ST-1 vehicle, the roll disturbance gave rise to erroneous radar tracking data that resulted in the prevention of the fourth-stage motor ignition. Highly unstable motors with cylindrical grain perforations are es-

pecially subject to roll-torque generation, although similar effects are exhibited in other complex grain configurations such as the star perforated cavities (ref. 2).

This investigation was conducted to determine which operating variables control the onset of transverse mode instability in solid-propellant motors and to compare the data with existing theoretical work. The results of an experimental program utilizing a two-dimensional vortex combustor are presented. Variations in the fundamental flame behavior of the propellant were made by changing the oxidizer particle size and the operating pressure. The resulting stability behavior of the motors, namely, the onset condition and duration of oscillation, was compared with stability boundaries based on a calculated response function of the propellant. These calculated response functions were made by assuming quasi-steady behavior of the propellant combustion. Energy release during pressure oscillation was assumed to be proportional to the burning rate that included both a pressure and an erosive velocity term. Wave amplification was achieved by biasing the tangential gas velocity, which resulted in a larger amount of energy addition during the high-pressure portion of the cycle than during the low-pressure portion.

Both solid (ref. 4) and liquid (ref. 5) motors have been driven unstable when high-pressure tangential nitrogen injection was used. In the present work, however, a ramping hot-gas generator supplied the gases required for driving the instability. The use of this particular configuration represents a new technique for driving a motor unstable in the transverse mode and offers the possibility of a new rating device for solid propellant instability in conjunction with current techniques (ref. 6). The preliminary experimental results obtained in this study have been reported previously (ref. 7) and are superceeded by this report.

SYMBOLS

A_B	motor propellant burning area, in.^{2}
A_t	motor throat area, in.^{2}
a	sound speed, ft/sec
B	constant (see eq. (7))
C	strand burning rate constant (see eq. (8))
C_p	specific heat at constant pressure
C_1	parameter equal to $(k\bar{\rho}a)^m/C\bar{P}^n$
C*	characteristic exhaust velocity, ft/sec
D	instantaneous inside diameter of propellant grain, in.

D_0	initial inside diameter of propellant grain, 5 in.
g	acceleration due to gravity, ft/sec^2
K	burning area to throat area ratio, A_B/A_t
k	erosion constant (see eq. (8))
$\dot{m}$	mass consumption rate, lb/sec
N	propellant response (see eq. (16))
P	chamber pressure, psia
R	motor radius, in.
r	propellant strand burning rate, in./sec
t	time, sec
Δt	finite time increment, 0.1 sec
V_{max}	magnitude of velocity vector in three component directions
v	mean gas velocity, ft/sec
w	energy release rate, ft-lb/sec
z	axial direction
α	swirl strength (see eq. (3))
γ	ratio of specific heats, 1.2
ϵ	amplitude factor (see eq. (10))
Γ	circulation
ρ	density, lb/ft^3

Subscripts:

eff	effective
f	final or propellant burnout
i	initial or ignition
m	maximum
pk-pk	peak to peak
s	solid phase
t	time
vor	vortexing flow condition

θ tangential direction

1 outermost radial position, outboard

2 second radial position

Superscripts:

n pressure exponent

m erosion exponent

* nozzle throat condition

– average value during oscillation

~ oscillating component in phase with pressure (see eq. (12))

APPARATUS AND PROCEDURE

Motor Design

The experimental combustor used in this study was composed of three parts, the main chamber, a gas generator, and an instability jet. The mode of operation is shown in figure 1(a), which illustrates the essential components of the vortex burner. A cross section of the assembled motor is shown in figure 1(b). The main chamber had a 9-inch outside diameter, a 7-inch inside diameter, and was 1/2 inch deep. Two polymethylmethacrylate windows were clamped to the top of the main chamber. Nitrogen at 250 pounds per square inch absolute was used to pressurize the space between the windows in order to prevent them from bowing during combustion. Visual and photographic observations were thus possible over the entire combustor cross section. The chamber and double window assembly were held together with two clamping rings by forty-eight 1/4-inch bolts. The bottom ring had two tabs, 180° apart, which were used for mounting the motor assembly. In the experimental testing, 12 motors were used.

The motors were designed to give a maximum pressure of approximately 45 pounds per square inch absolute with radial burning, that is, in the absence of tangential flow to the propellant surface. The throat-diameter motor used was 1/2 inch. Tests were also conducted with a 3/4-inch diameter throat motor that yielded an unchoked condition with radial burning only.

Gas Generator and Instability Jet

The gas generator (fig. 1(c)), was a brass cup 1/2 inch deep by 2 inches in inside

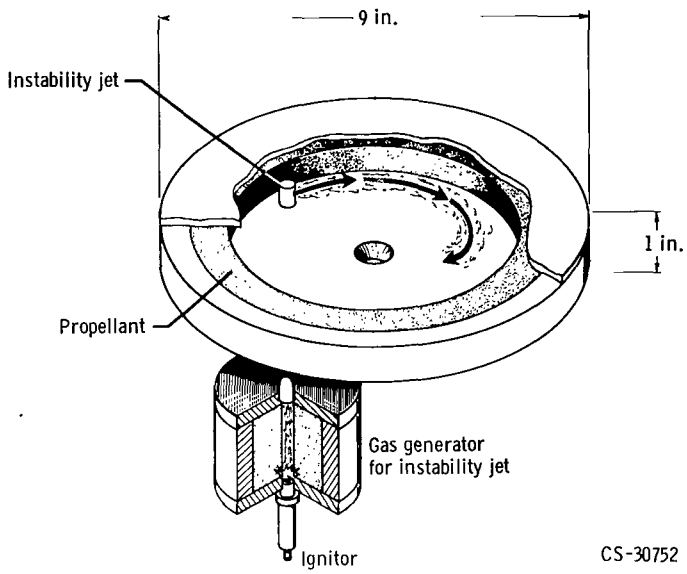

(a) Experimental geometry and mode of operation.

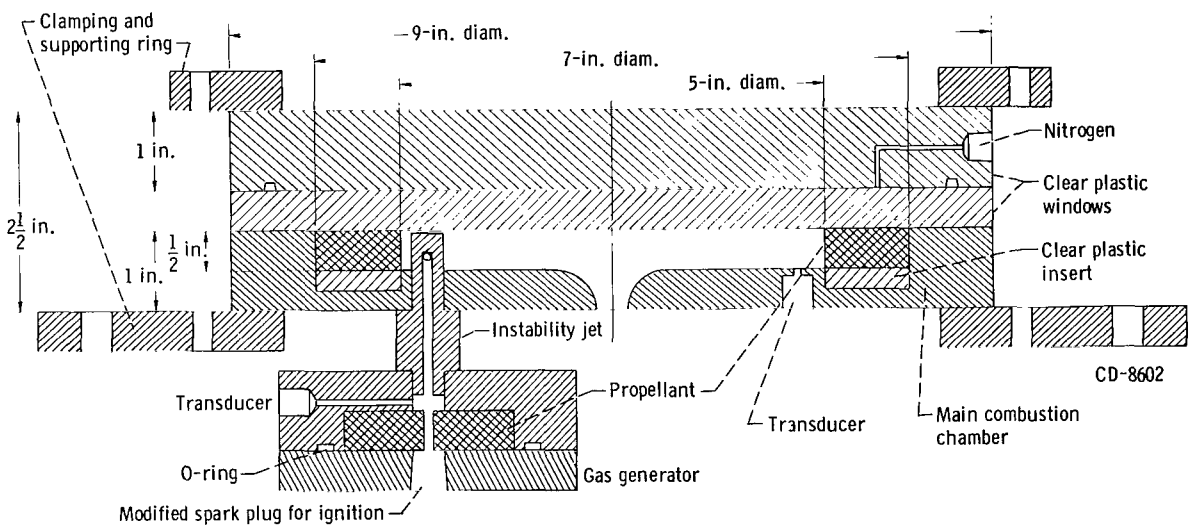

(b) Motor, gas generator, and instability jet assembly.

Figure 1. - Experimental combustor.

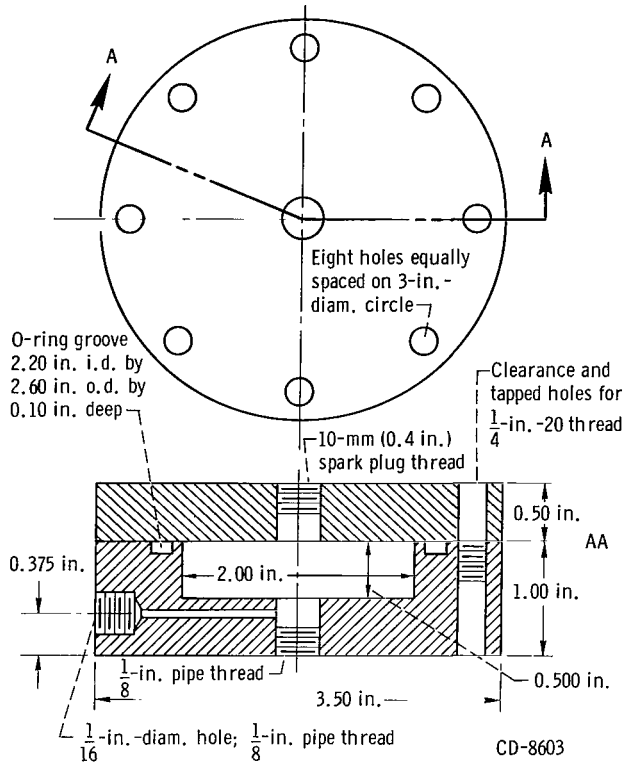

(c) Gas generator details; material, brass.

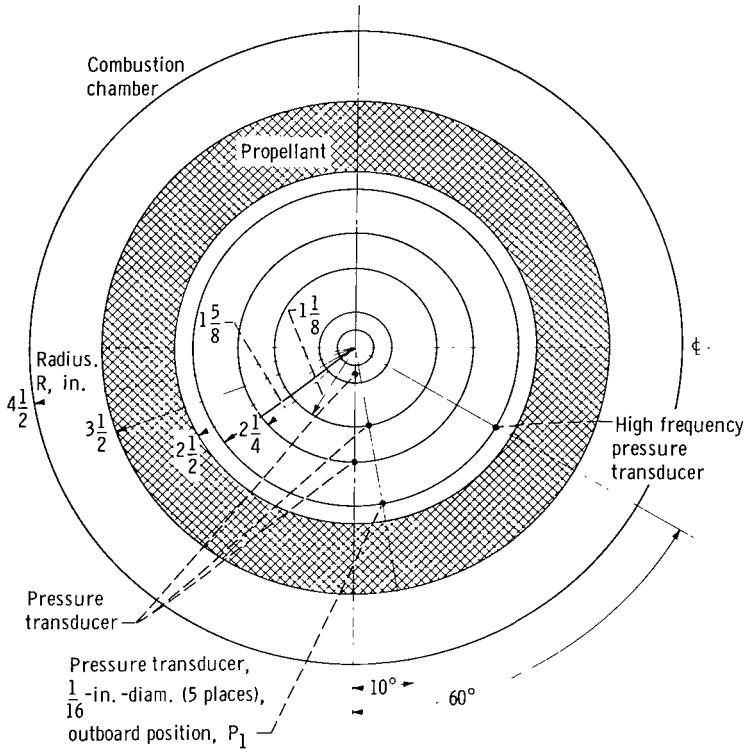

(d) Typical pressure transducer locations.

Figure 1. - Continued.

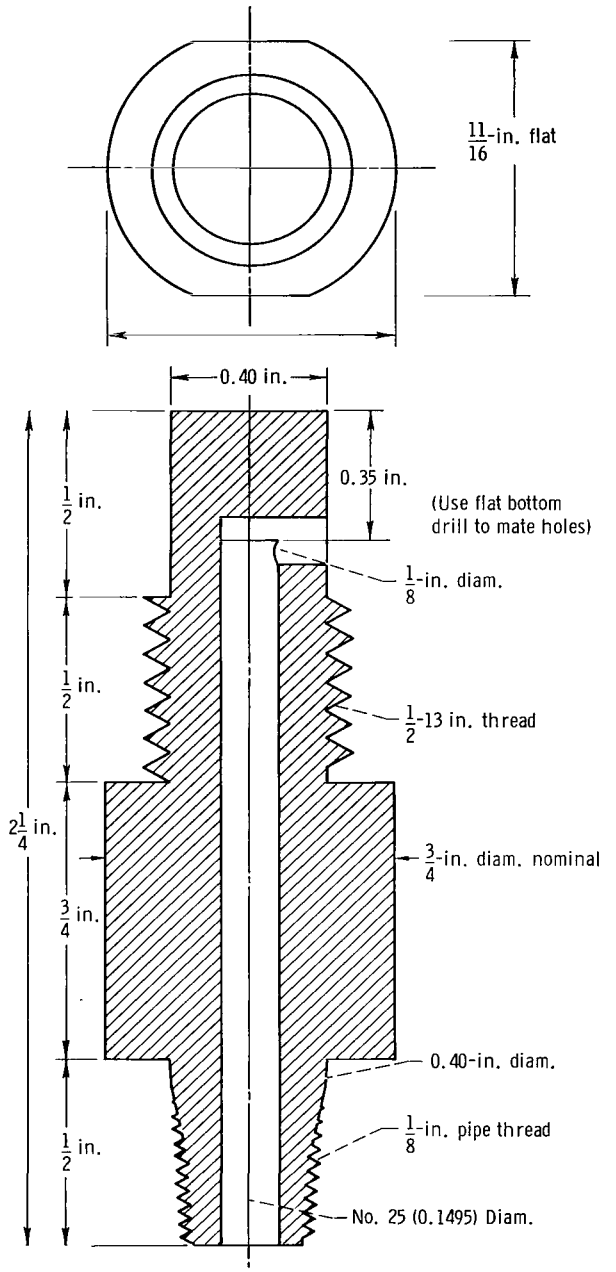

(e) Instability jet design; material, copper.

Figure 1. - Concluded.

diameter filled with solid propellant by direct casting. The top surface of the propellant was machined flat and left 1/16 inch higher than the generator surface. A cover, bolted into place, compressed the propellant and proved effective in preventing combustion at the grain-wall interface. A center hole, 1/4 inch in diameter, was drilled through the propellant grain from the top to the bottom surface. A modified spark plug with an extended center electrode, a short length of fuse, and explosive wire was threaded into the bottom of the generator as an ignition source. The progressive combustion characteristic of the gas generator yielded a slowly ramping pressure-time trace that was quite reproducible. Pressure transducer locations are shown in figures 1(b) to (d). The generated gases passed through an opening in the top cover into the instability jet (fig. 1(e)). The direction of the injected generator gases in the main chamber was tangent to the propellant surface at a point on the circumference. The hot injected gases served two purposes, namely, to ignite the propellant in the main chamber and to introduce a tangential gas flow (whose flow magnitude increased with time).

Propellant

The propellant in the main chamber, 5 inches in inside diameter, 7 inches in outside diameter by 1/2 inch thick, was cast into place above an expandable polymethylmethacrylate ring. The propellant was then cured for 18 hours. The top surface of the propellant was machined flat and left 1/8 inch

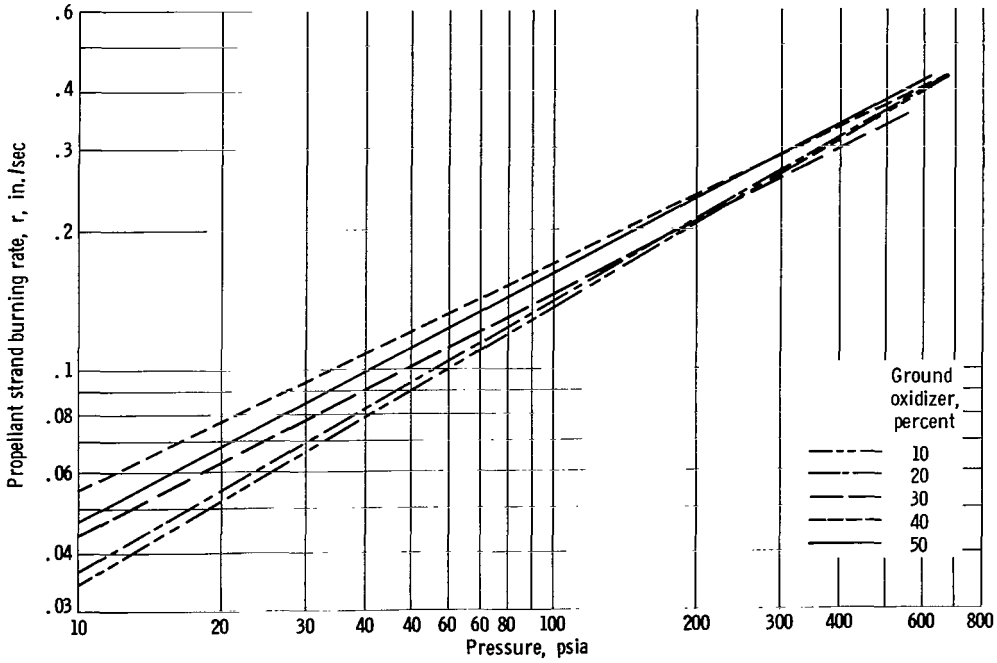

Figure 2. - Propellant strand burning rate data. Material, 81 percent ammonium perchlorate and 19 percent polybutadiene acrylic acid.

higher than the motor surface. The inside diameter of the propellant grain was also machined to give a uniform surface. Clamping the double window section made a tight fit of the grain between the Plexiglas surfaces which prevented combustion on the top surface of the propellant to operating pressures of approximately 300 pounds per square inch absolute.

The propellants used in this study were composed of ammonium perchlorate and polybutadiene acrylic acid, 81 and 19 percent be weight, respectively. The oxidizer was a blend of ground (11μ mean weight diameter) and unground (85μ mean weight diameter) crystals. The particle size distributions are given in reference 8. The percent ground oxidizer used in the main chamber was 10, 20, 30, 40, and 50 percent. The generator propellant had 30-percent ground oxidizer and was not varied. The linear regression rates of the propellants are shown in figure 2.

Instrumentation

Pressure transducers were located at various radial positions in the main chamber ranging from a point directly over the nozzle center (fig. 1(b)) to a point close to the initial propellant burning surface (fig. 1(d)). A high-frequency crystal transducer was also located at the outermost radial position. Pressure measurements made at this location are hereinafter referred to as outboard pressure and designated P_1. The gas generator was also instrumented with a pressure transducer. Both cooled and uncooled high-frequency transducers were used throughout the 108 experimental tests. Recess mounting

was used with the uncooled transducer, whereas the cooled transducers were flush mounted. The output of the transducers was recorded directly on magnetic tape.

Both low-speed and high-speed framing (600 and 4000 fps, respectively) cameras were used to record the motor test through the window section of the main chamber. A program timer was used to give a regular sequence of events. The operating sequence was arranged so that the low-speed camera would begin at the start, followed by gas generator ignition 1/2 second later, and then by the high-speed camera 3 to 5 seconds from the start. A function signal of 60 cycles per second whose amplitude varied with the closing of the individual timing channels was recorded on tape simultaneously with the transducer output. The test was also monitored on a recording oscillograph and manually marked at the time of full flame around the combustor and at the end of the vortexing flow (gas-generator burnout).

A variable resistor connected into a 115-volt line and set at 40 volts was used to energize the spark plug in the gas generator. Combustion gases flowing into the main chamber ignited the propellant after a short time delay. Burning was restricted to the inside circumference of the propellant only.

RESULTS AND DISCUSSION

Pressure-Time Behavior

The increase of burning area within the gas generator yielded a gradually increasing pressure (fig. 3). The corresponding change in the outboard pressure P_1 of the main

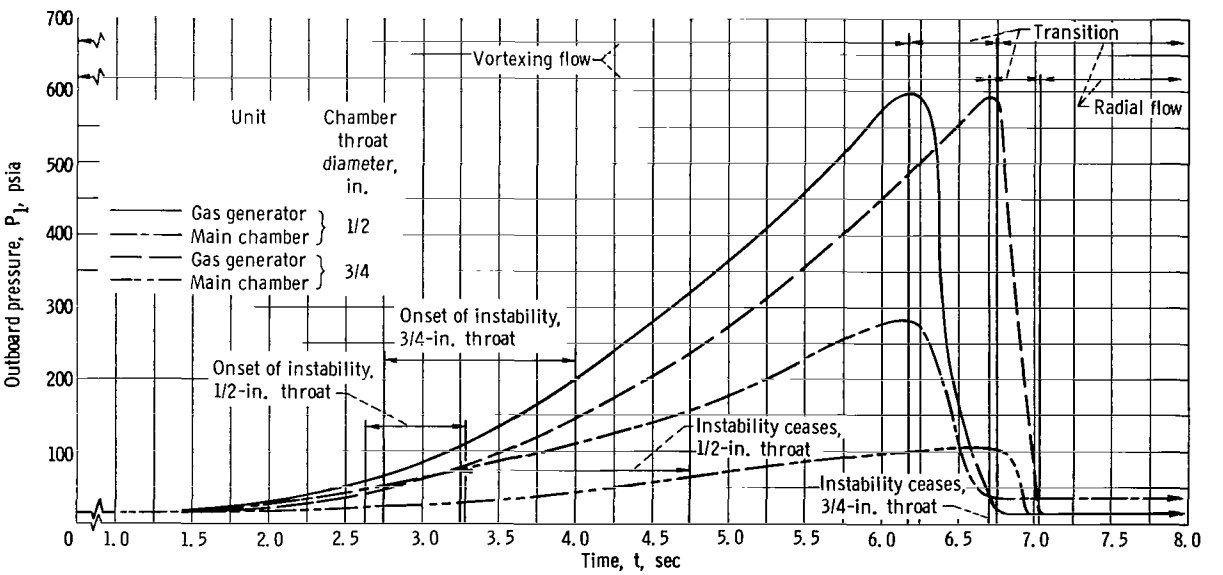

Figure 3. - Pressure-time behavior of gas generator and main chamber.

chamber, shown for the motor with 1/2- and 3/4-inch-throat diameters, follows the generator output quite closely. The flow field within the motor was primarily tangential relative to the burning propellant surface and gradually increased in magnitude for about 6 seconds after which the generator ceased burning. Following generator burnout, the unconsumed propellant continued to burn in the low-pressure environment. The flow during this remaining portion of the test quickly changed to the radial direction toward the nozzle entrance. Figure 4 shows the flame behavior during the vortexing and radial flow portions of the run. The maximum pressure developed in the 1/2-inch-throat diameter was 285 pounds per square inch absolute. In the absence of tangential flow, the maximum operating pressure was experimentally observed to be 35 pounds per square inch absolute, whereas the calculated design pressure was 45 pounds per square inch absolute. For the motor with 3/4-inch-throat diameters, that would operate unchoked without tangential flow, the maximum pressure was 105 pounds per square inch absolute. These large increases in motor chamber pressure were caused mainly by (1) addition of mass from the gas generator, (2) erosive burning due to the high tangential velocities in the main chamber, and (3) reduction of the effective nozzle-throat area due to vortexing flow in the vicinity of the nozzle. Each of these causes is discussed in the following sections. As will be shown, it is the third effect, namely, the vortexing phenomenon in the nozzle, that is primarily responsible for the large increases in chamber pressure. The results of figure 3 are typical of all propellants used and for both nozzle diameters. Hence, these curves will be used in all subsequent calculations.

Generator Mass Addition

The increase in motor chamber pressure due to the addition of the mass of the gas generator may be determined from the product of the generator pressure and the ratio of the jet exit area to the motor throat area (if a constant C^* is assumed). By using a peak generator pressure of 550 pounds per square inch absolute, an increase of 34 pounds per square inch absolute was calculated for the 1/2-inch-throat motor. This value was verified experimentally by firing the gas generator radially into an empty motor. The maximum pressure expected, therefore, was about 80 pounds per square inch absolute plus a slight increase (5 to 10 psia) due to the adjustment of the increased rate of the burning in the motor since the burning rate is pressure sensitive. Hence, the equilibrium pressure was slightly higher than that pressure due to generator mass addition only.

(a) Vortexing flow.

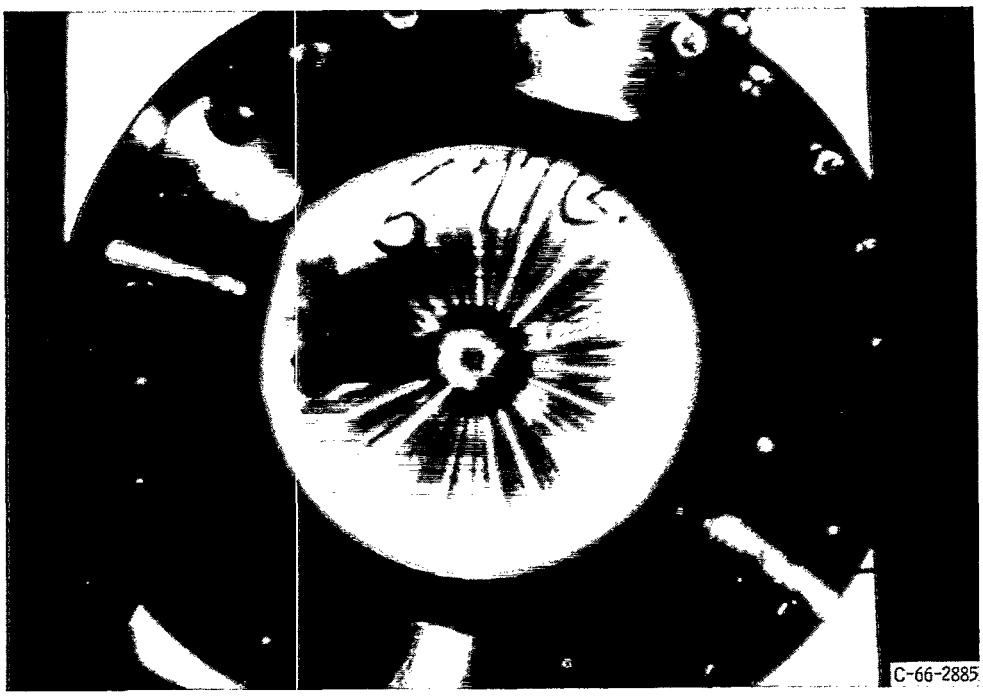

(b) Radial flow.

Figure 4. - Direct photograph of motor firing.

TABLE I. - DIAMETER-TIME HISTORY FOR 3/4-INCH-DIAMETER-THROAT MOTOR

Time, t, sec	Chamber pressure, p_c, psia	Gas generator pressure, P_{gg}, psia	Propellant burning rate, r, in. /sec	Modified instantaneous diameter, D + r/5, in.	Erosive calculation			
					4 percent increase in r, r_1, in.	Instantaneous diameter, D, in.	10 percent increase in r, r_2, in.	Instantaneous diameter, D, in.
2.3	21.7	35.0	0.056	5.00	0.058	5.00	0.064	5.00
2.4	21.7	35.0	.056	5.01	.058	5.012	.064	5.013
2.5	21.7	35.0	.056	5.02	.058	5.024	.064	5.026
2.6	21.7	41.7	.056	5.03	.058	5.036	.064	5.039
2.7	25.0	48.4	.060	5.042	.063	5.049	.069	5.053
2.8	25.0	48.4	.060	5.054	.063	5.062	.069	5.067
2.9	25.0	55.1	.060	5.066	.063	5.075	.069	5.081
3.0	28.4	61.0	.065	5.079	.067	5.088	.074	5.096
3.1	28.4	68.4	.065	5.092	.067	5.103	.074	5.111
3.2	28.4	68.4	.065	5.105	.067	5.116	.074	5.126
3.3	28.4	75.1	.065	5.118	.067	5.129	.074	5.141
3.4	28.4	81.8	.064	5.131	.067	5.142	.074	5.156
3.5	31.7	95.2	.068	5.145	.070	5.156	.077	5.161
3.6	35.0	101.8	.072	5.159	.076	5.171	.084	5.178
3.7	38.4	108.5	.076	5.174	.080	5.187	.088	5.196
3.8	38.4	125.2	.076	5.189	.080	5.203	.088	5.214
3.9	41.7	135.2	.080	5.205	.084	5.220	.092	5.232
4.0	43.7	148.6	.082	5.221	.086	5.237	.095	5.251
4.1	45.1	151.9	.082	5.237	.088	5.255	.097	5.270
4.2	45.1	162.0	.083	5.253	.088	5.273	.097	5.289
4.3	51.7	175.3	.091	5.271	.096	5.292	.150	5.319
4.4	55.1	195.4	.094	5.290	.100	5.312	.110	5.341
4.5	58.4	208.7	.097	5.310	.103	5.332	.113	5.363
4.6	60.1	212.1	.099	5.330	.105	5.351	.115	5.386
4.7	63.4	235.4	.101	5.350	.108	5.373	.118	5.409
4.8	61.8	245.5	.100	5.370	.106	5.393	.116	5.432
4.9	63.4	258.8	.101	5.390	.108	5.415	.118	5.455
5.0	71.8	275.5	.109	5.412	.116	5.438	.127	5.480
5.1	78.5	292.2	.115	5.435	.123	5.462	.135	5.507
5.2	81.8	302.2	.118	5.459	.125	5.487	.138	5.534
5.3	83.5	322.0	.119	5.483	.127	5.512	.140	5.562
5.4	83.5	335.6	.119	5.507	.127	5.537	.140	5.590
5.5	85.1	359.0	.120	5.531	.128	5.563	.141	5.618
5.6	88.5	372.4	.123	5.556	.131	5.589	.144	5.647
5.7	90.2	395.8	.123	5.581	.133	5.615	.147	5.677
5.8	88.5	412.5	.121	5.601	.131	5.641	.144	5.706
5.9	85.1	429.2	.118	5.625	.128	5.667	.141	5.734
6.0	91.8	449.2	.123	5.640	.135	5.694	.149	5.764
6.1	91.8	472.6	.123	5.665	.135	5.721	.149	5.794
6.2	95.2	489.3	.125	5.690	.137	5.748	.151	5 824
6.3	95.2	506.0	.125	5.715	.137	5.775	.151	5.854
6.4	95.2	526.0	.125	5.735	.137	5.802	.151	5.884
6.5	98.5	553.0	.126	5.755	.140	5.830	.154	5.914
6.6	103.5	569.0	.130	5.781	.145	5.859	.160	5.946
6.7	105.2	593.0	.131	5.807	.145	5.888	.160	5.978
6.8	121.9	526.0	.148	5.836	.158	5.920	.174	6.013
6.9	60.1	279.0	.096	5.855	.105	5.941	.115	6.036
7.0	28.4	91.8	.064	5.870	.067	5.954	.074	6.051
7.5	15.0	15.0	.046	-----	.047	6.001	.051	6.061

Erosive Burning

A further explanation for the increased pressure may be a result of the effect of the tangential velocity on the propellant burning rate. By using the recorded pressure-time trace for the 3/4-inch-diameter throat motor (fig. 3, p. 9) the instantaneous diameter of the propellant grain in the absence of erosive burning may be calculated at any time by suitable integration of the strand burning rate over small time intervals. Adding the initial inside diameter of the propellant grain gives

$$D = D_0 + 2\,\Delta t \sum_{t_i}^{t_f} r_t \qquad (1)$$

By using a time interval of 0.10 second, the instantaneous diameter of the propellant was determined throughout the entire test. These calculations are presented for the 3/4-inch-diameter throat motor in table I. The inside diameter of the propellant grain at generator burnout was calculated to be 5.87 inches. After generator burnout, this motor continued to burn for 13.4 seconds at atmospheric pressure. Since the strand propellant burning rate was 0.046 inch per second at atmospheric pressure (fig. 2, p. 8), the radial distance burned during the nonvortexing or radial flow portion of the run was 0.616 inch. The inner diameter of the propellant grain at generator burnout was, therefore, equal to the outside diameter of the grain minus 2 times 0.616 inch or 5.77 inches. Comparison of this value of the grain diameter with that determined by using the finite difference technique revealed good agreement (a difference of 0.10 in. inside diameter). The propellant diameter time history with vortex motion, therefore, can be closely predicted by using the strand burning rate. Additional calculations were made by using equation (1) and assuming approximate increases of 5 and 10 percent in the strand burning rate (see table I). This yielded inner diameters of 5.98 and 6.05 inches, respectively, which also were in reasonable agreement with 5.77 inches determined previously. Calculations performed on the 1/2-inch-throat motor with various propellant compositions also revealed good agreement. Hence, it was concluded that the amount of erosive burning that occurred during the motor firings did not exceed 10 percent. The data do not warrant a more accurate statement. Direct photographic measurement of the erosive burning rate was not possible because of insufficient accuracy. These data supersede the data of reference 7.

The maximum motor pressure expected including erosion was calculated by assuming that the strand burning curve was 10 percent higher at 200 pounds per square inch absolute, whereas the intercept (1 psia) remained fixed (fig. 2). The maximum pressure calculated for the 1/2-inch-diameter throat motor was

$$P = \left(\frac{K\rho_s CC^*}{g}\right)^{1/(1-n)} = 60 \text{ psia} \qquad (2)$$

Addition of the generator flow would raise the maximum pressure to a value of only 100 pounds per square inch absolute.

Vortex Effect on Nozzle Flow

The remaining cause of excessive motor pressure was a result of nozzle throat constriction caused by the vortexing flow as it passes through the nozzle. In reference 9, a theory was developed for calculating the increase in chamber pressure due to the presence of a vortex. Use of this one-dimensional theory for vortex flow through a nozzle has shown a large reduction in the mass flow and axial Mach number as the swirl stength is increased (fig. 5 and ref. 4). The swirl strength α is defined as

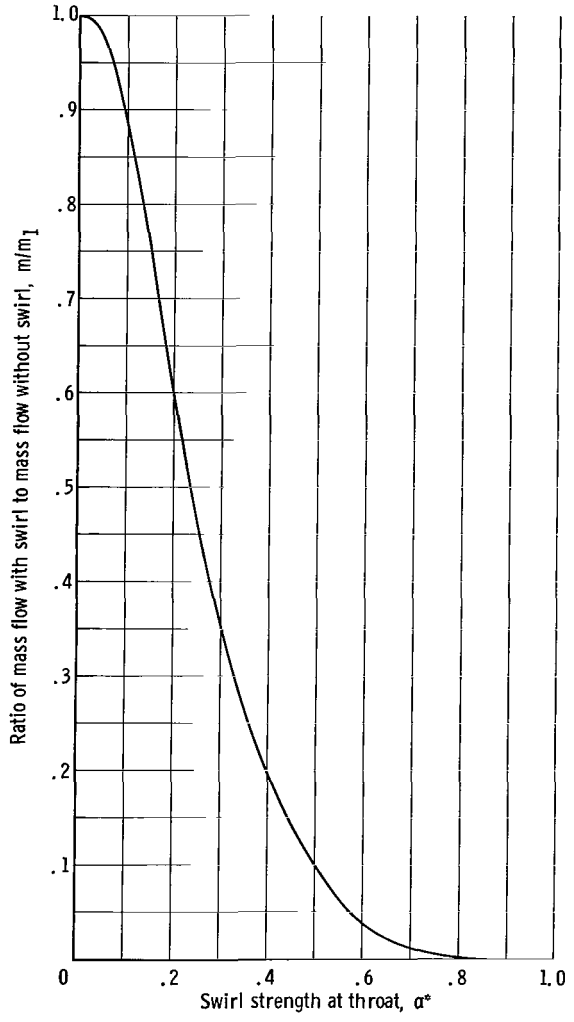

Figure 5. - Effect of swirl strength on mass flow at constant chamber pressure (ref. 4).

$$\alpha = \frac{\overline{v}_\theta}{V_{max}} \qquad (3)$$

where V_{max} is the magnitude of the velocity vector in the three component directions, and $\overline{v}_\theta$ is the tangential velocity at the wall. Hence, at high values of $\overline{v}_\theta$, the effective nozzle-throat area is reduced, which leads to high chamber pressures. Calculations of the swirl strength for the motors in the present study were made by using $\overline{v}_\theta$ values (determined from radial pressure measurements given in a later section) and the conservation of angular momentum, namely,

$$\alpha^* = \alpha \frac{R}{R^*} \qquad (4)$$

where the star denotes conditions at the nozzle throat, and R^* is the throat radius. The values of α^* for the motors in this study were close to 1, and, hence, the effective throat area should approach zero, and the chamber pressure should rise to an infinite value. Obviously, the one-dimensional theory does not adequately describe the vortex flow in the nozzle and cannot be used for determining the increase in chamber pressure in the present experiments.

A rough estimate of the effective throat diameter was obtained by running the motor both with and without vortex flow and evaluating the following expression

$$A_{t,\,eff} = A_t \frac{\dot{m}_{vor}}{\dot{m}} \frac{\int_0^{t_f} P\,dt}{\int_0^{t_f} P_{vor}\,dt} \tag{5}$$

where C^*_{vor} was assumed equal to C^*. The total mass of propellant burned amounted to 0.7 pound - 0.6 pound in the main chamber and 0.1 pound in the gas generator. The value of the ratio of integrals in equation (5) was approximately 0.2, that is, $\int_0^{t_f} P\,dt = 3.6$, and $\int_0^{t_f} P_{vor}\,dt = 18$. Some difficulty was encountered in evaluating the area under the pressure-time trace for the nonvortexing case because of the long, slowly rising low-pressure portion of the run. The preceding values gave a calculated effective throat diameter of 0.25 inch compared with the real throat diameter of 0.50 inch. The effect of swirl, with some contribution from generator mass addition and erosive burning, was to reduce the effective nozzle diameter by approximately 50 percent.

A further set of experiments was run in order to confirm the strong influence of the vortex flow on the large rise in chamber pressure. The experiments were conducted with the same motor geometry used previously, with a single exception. A 1/8-inch-thick ring with radially drilled holes was used (fig. 6). Three ring diameters used were $3\frac{1}{2}$, $2\frac{3}{8}$, and

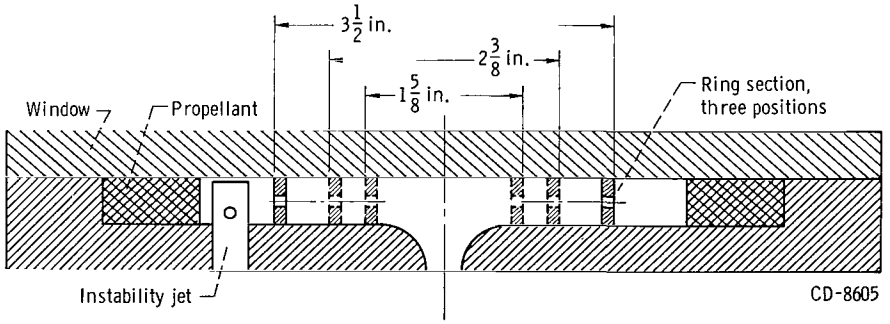

Figure 6. - Motor geometry with damping ring.

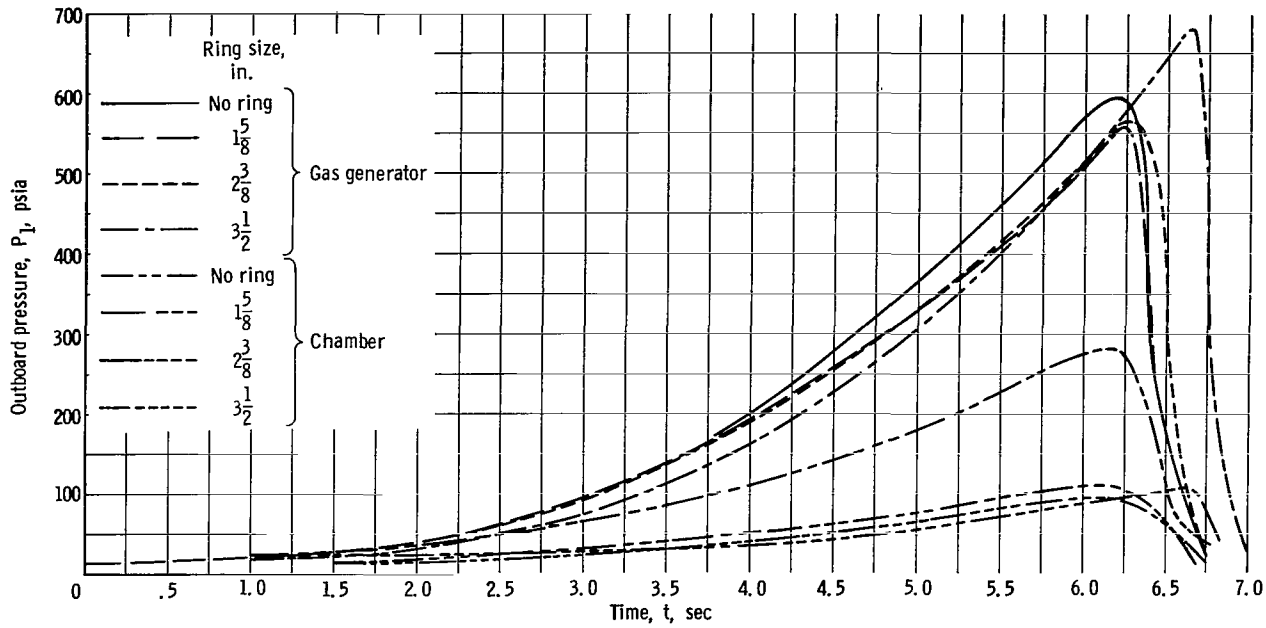

Figure 7. - Pressure-time trace. Chamber throat diameter, 1/2 inch.

$1\frac{5}{8}$ inches. Approximately 35 holes were drilled in the ring sections to give a flow area greater than the nozzle throat area. Figure 7 shows the results obtained with the 1/2-inch-diameter throat motor. The maximum outboard pressure was substantially lower than the no-ring case. This maximum pressure, 100 pounds per square inch absolute, corresponds to that calculated previously where mass addition from the gas generator and erosion were included. It appears, therefore, that the ring prevented the formation of a vortex flow (i. e., large pressure distribution) within the motor; hence, the effective nozzle area remained equal to the real nozzle area. The presence of the ring served to straighten the flow before reaching the nozzle. The nozzle blockage effect due to swirling flow was, therefore, eliminated, and there were no large pressure increases. Regardless of the three ring positions, the nozzle flow blockage effect of the swirling flow was eliminated, which prevented the chamber pressure from rising to values obtained with the unbaffled motors.

Figure 8 shows similar results for the 3/4-inch-diameter throat motor where the maximum chamber pressure reached only 50 pounds per square inch absolute. Again, this value corresponds approximately to what would be expected with generator mass addition and a small amount of erosive burning. Use of the ring also prevented the excessive rise due to the nozzle blockage effect. These results verified that the main cause of high-chamber pressure was a result of the vortex flow in the combustor.

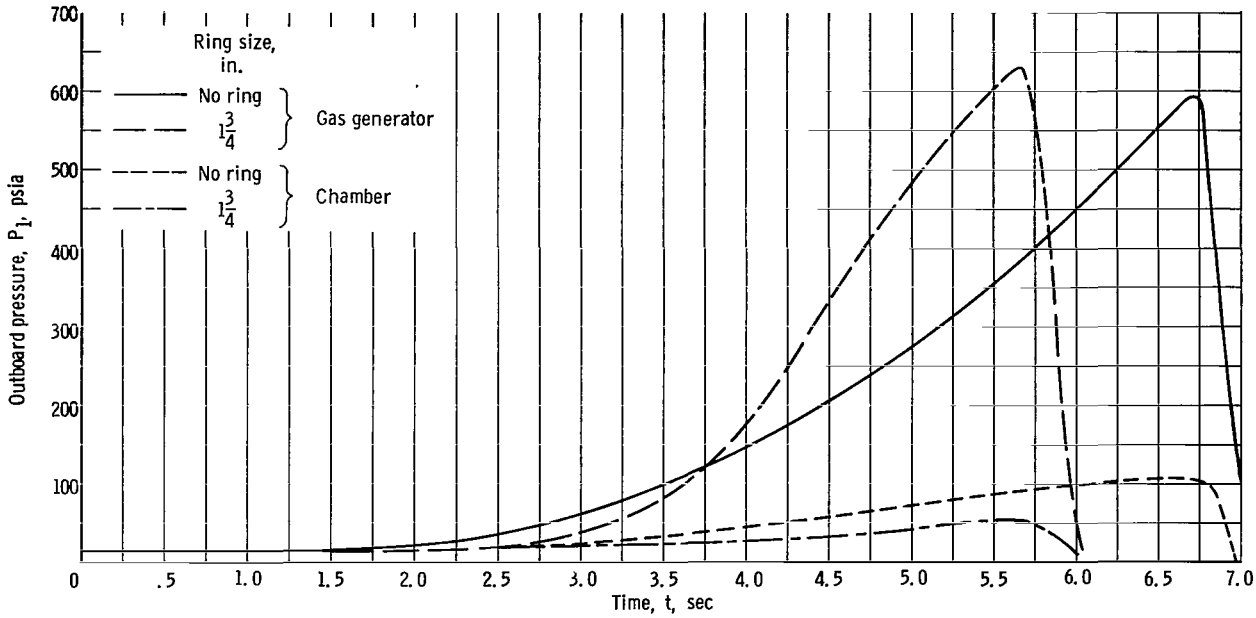

Figure 8. - Pressure-time behavior. Chamber throat diameter, 3/4 inch.

Instability Characteristics

The onset of combustion instability occurred at some time during the firing as the pressure was rising (fig. 3, p. 9). For the 3/4-inch-throat diameter, the instability continued until gas generator burnout occurred, whereas with the 1/2-inch-throat diameter the pressure oscillations ceased somewhere between 1/2 to 1 second following the onset of instability. A few runs with a 5/8-inch-diameter throat motor showed the onset pressure to be intermediate between the 1/2- and 3/4-inch diameter throat motors (fig. 9). The duration of the instability was slightly longer than that in the 1/2-inch motor. This onset pressure, which did not appear to be dependent on the percentage of ground oxidizer in the propellant, increased with increasing burning area to throat area $K_i = A_B/A_t$ which is a typical correlating parameter for solid-propellant motor instability. The corresponding propellant strand burning rates (fig. 2, p. 8) at the onset of instability gives the results shown in figure 10. A higher burning rate was required for instability with increasing burning area to throat area ratio K_i. These plots show some dependence on the ratio K_i but do not give much insight into the occurrence of instability. In addition, the propellant compositions used herein do not appear to have any influence on the initiation of instability. It is necessary to look in greater detail at the oscillatory behavior.

The amplitude of the pressure oscillations for both motors are shown in figures 11 and 12 as a function of the propellant composition (percent ground oxidizer) and the motor test time. The amplitude remained fairly constant with oxidizer particle size for

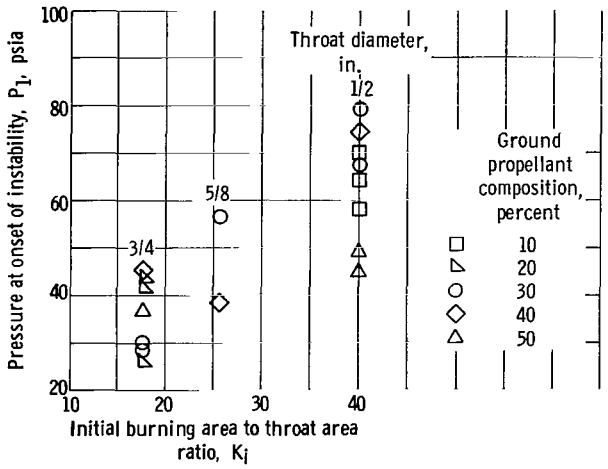

Figure 9. - Onset pressure as function of burning area to throat area ratio.

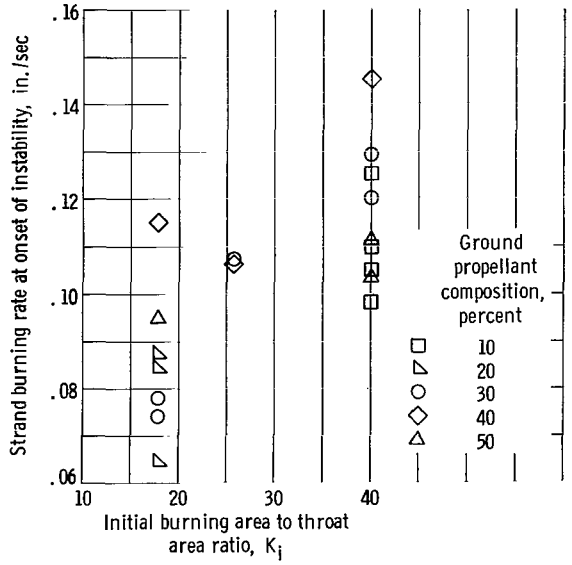

Figure 10. - Strand burning rate at onset of instability as function of burning area to throat area ratio.

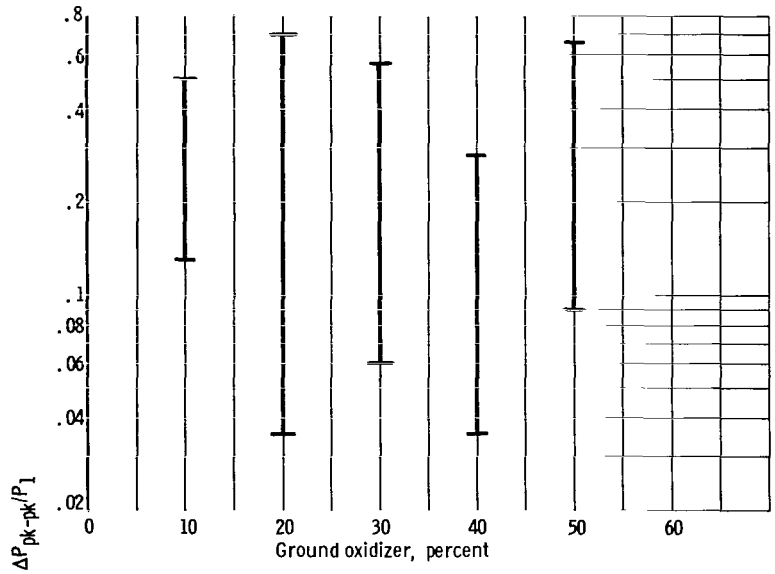

(a) Amplitude as function of ground oxidizer.

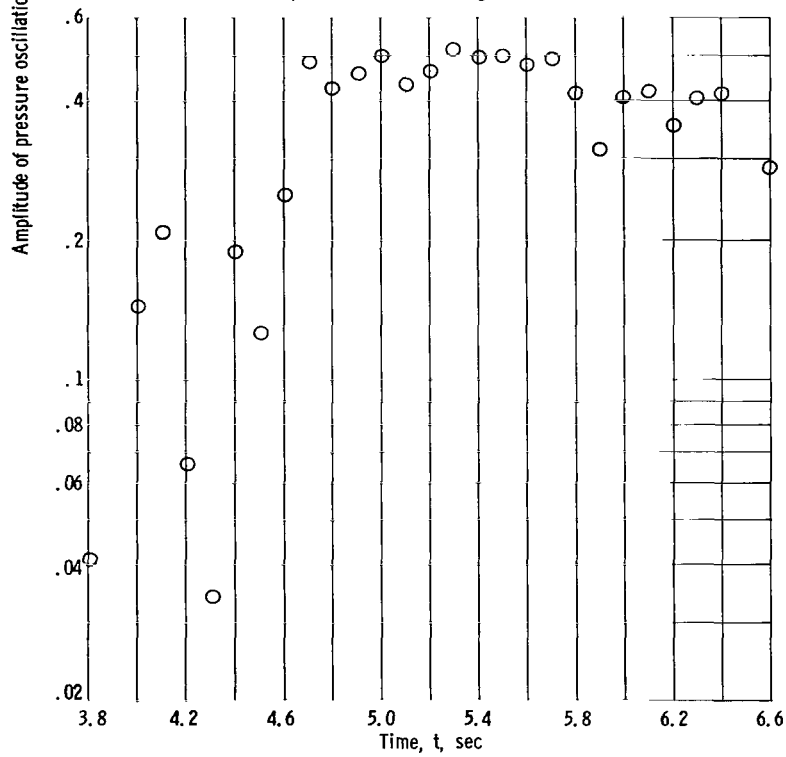

(b) Amplitude as function of time. Throat diameter, 3/4 inch; ground oxidizer, 20 percent.

Figure 11. - Peak-to-peak pressure oscillations for 3/4-inch diameter throat motor.

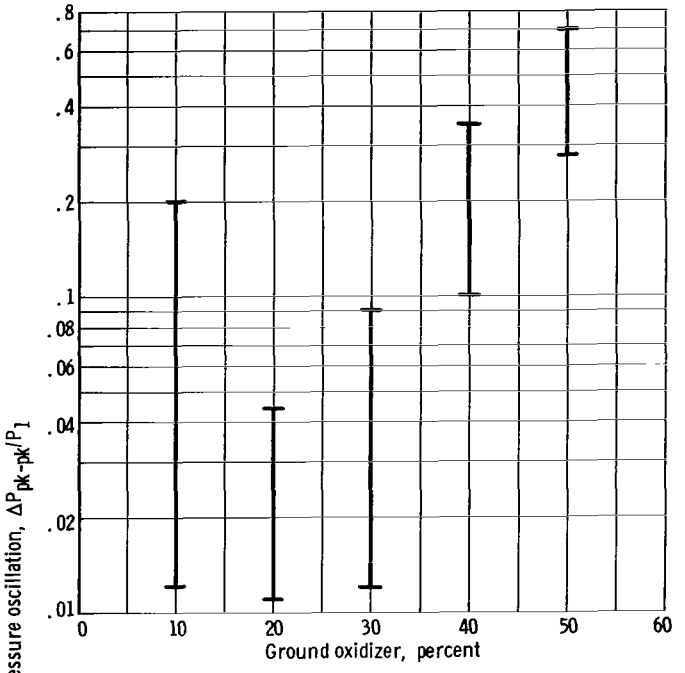

(a) Amplitude as function of ground oxidizer.

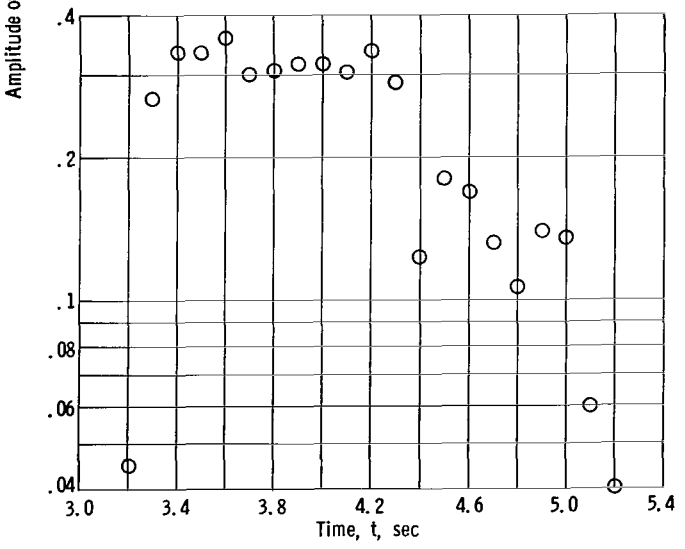

(b) Amplitude as function of time. Ground oxidizer, 40 percent.

Figure 12. - Peak-to-peak pressure oscillations for 1/2-inch diameter throat motor.

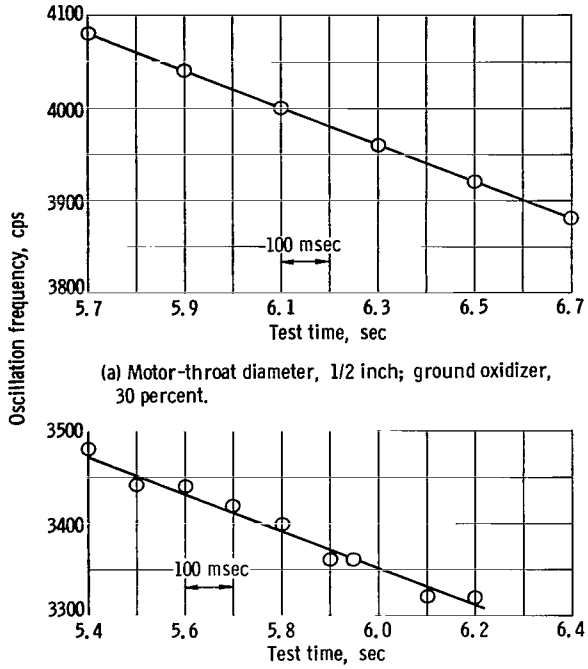

(a) Motor-throat diameter, 1/2 inch; ground oxidizer, 30 percent.

(b) Motor-throat diameter, 3/4 inch; ground oxidizer, 40 percent.

Figure 13. - Variation of frequency during test.

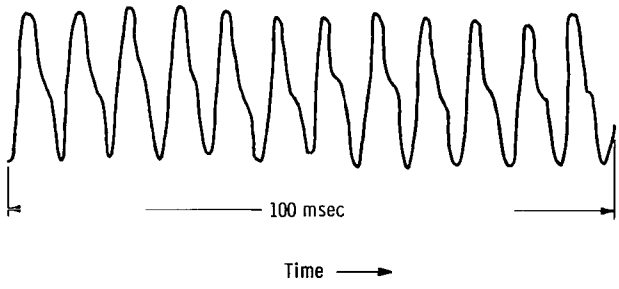

Figure 14. - Chamber-pressure wave shape. Ground oxidizer, 50 percent; throat diameter, 1/2 inch; direct current chamber pressure, 200 pounds per square inch; oscillation frequency, 3840 cycles per second; playback ratio, 32.

the 3/4-inch motor (fig. 11(a)), but showed a significant dependency in the 1/2-inch motor (fig. 12(a)). In both cases, the amplitude rose quickly to some value and exhibited a tendency to level off and remain fairly constant until the oscillation decayed (figs. 11(b) and 12(b)). Growth or decay constants were not calculated. Measurements of the amplitude of the oscillations below approximately 7 percent probably reflects the noise level in the combustor. The increase in amplitude as the percent ground oxidizer was changed from 20 to 50 percent, however, appears to be a real effect (fig. 12(a)). The high amplitudes exhibited by the 10-percent ground oxidizer is somewhat uncertain. Previous measurements in a T-motor at Lewis (ref. 10) by using the identical propellants showed similar behavior, namely, the oscillation amplitude increased markedly with the percent ground oxidizer in the propellant.

Since the inside diameter of the propellant grain increased with time, the oscillation frequency decreased with run time. This variation is shown in figure 13. The frequency of the oscillation corresponded to the first traveling transverse mode. Uniform erosion of the propellant grain around the circumference as well as the enhanced zone of luminosity moving around the combustor (observed by high-speed cameras) confirmed the mode of oscillation. A typical wave shape of the chamber pressure (fig. 14) revealed a fairly steep wave front with a distortion on the trailing side. The presence of this distortion was apparently a result of an interaction with, or reflection from, the instability jet located in the swirling flow stream. Changing the circular cross section of the jet injector to a streamline shape resulted in a significant decrease in the amount of distortion and tended to give a symmetrical wave shape. High-frequency transducers did not indicate any oscillation in the gas generator.

Erosion Patterns

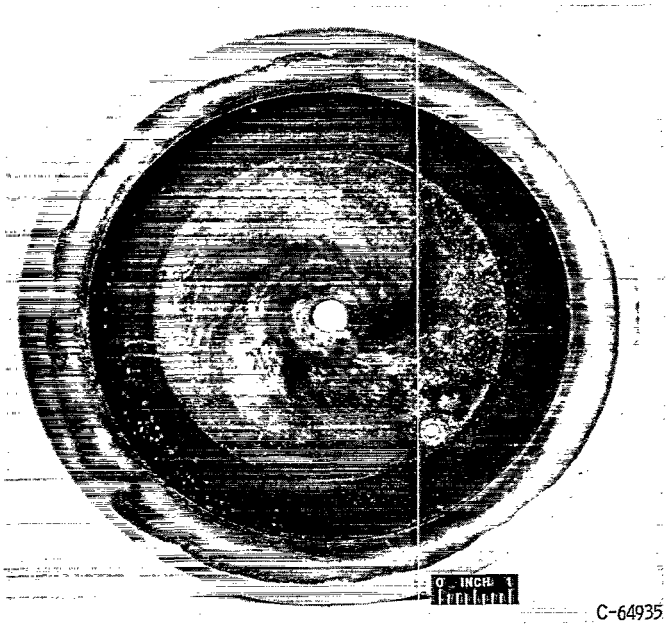

Figure 15. - Motor subsequent to firing.

Figure 15 shows the resulting flow patterns left on the bottom surface of the combustion chamber. The darker outside ring indicates the location of the propellant grain. The pattern on the center of the upper window directly above the nozzle center is shown in figure 16. A region, about 1 inch in diameter, was eroded to a greater depth than the surrounding portion of the window. In addition, window pitting occurred over a 1/2-inch diameter and can be observed in the photograph as a series of small craters about 1/16 inch deep. The very center of the window had a raised point. The presence of these erosion patterns was probably a result

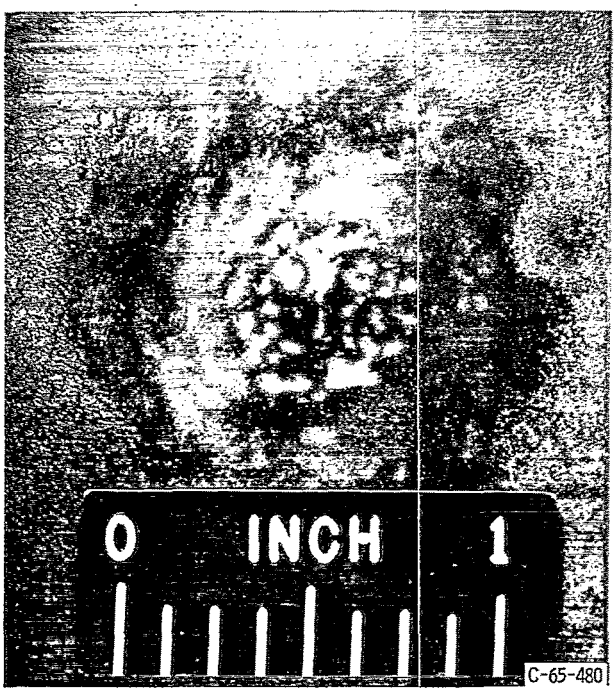

(a) Motor-thoat diameter, 1/2-inch.

(b) Motor-throat diameter, 3/4-inch.

Figure 16. - Erosion pattern at center of top window.

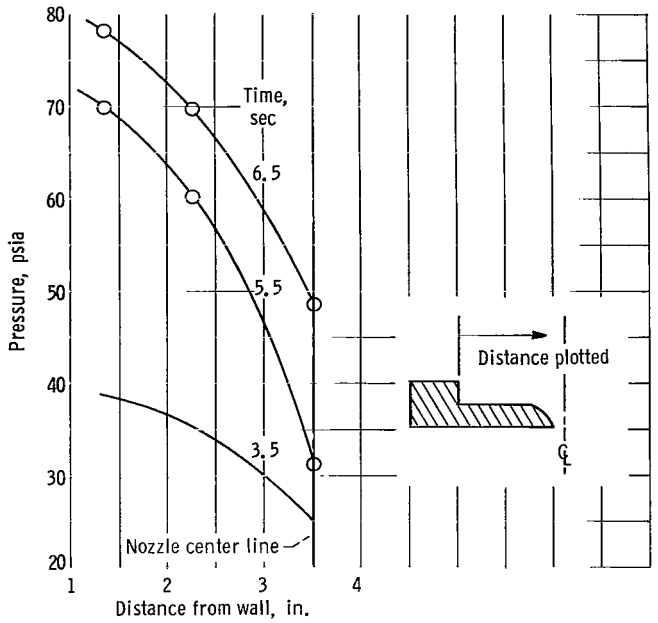

Figure 17. - Radial pressure measurement with vortex flow. Motor-throat diameter, 3/4 inch; ground propellant, 20 percent.

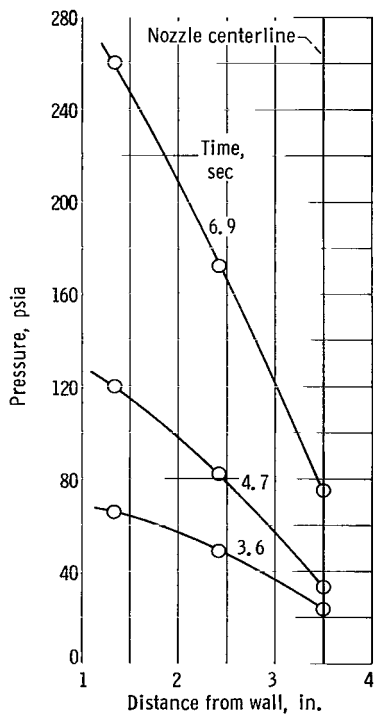

Figure 18. - Radial pressure measurement with vortex flow. Motor-throat diameter, 1/2 inch; ground propellant, 30 percent.

of the strong vortex flow field within the combustor. In order to define this flow more exactly, the pressure distribution in the engine was examined.

Radial Pressure Measurements in Combustor Flow Field

Pressure data obtained at the nominal radial positions (see fig. 1(d), p. 6) revealed the presence of strong radial pressure gradients, as shown in figures 17 and 18, at various times during the motor firings with vortex flow. All pressure measurements were made on the bottom wall of the combustor with the exception of the measurement at the nozzle center, which was made through the top window. Presence of a radial pressure distribution significantly alters the calculated values of the erosive burning as reported previously (ref. 7). On the basis of the strong pressure gradients existing in the motors, the flow field in the motors are believed to consist primarily of a free vortex. Tracing the flow pattern in an incompressible vortex (ref. 11) has shown the existence of strong secondary flows existing along the longitudinal axis of the combustor (fig. 19(a)). The existence of secondary flows has also been discussed for vortex flow through a rocket nozzle (ref. 12) and the presence of an elongated toroidal vortex postulated. The flow field in the motors of this study is shown in figure 19(b), and it is believed to consist of a strong vortex with secondary flow along the longitudinal axis of the motor.

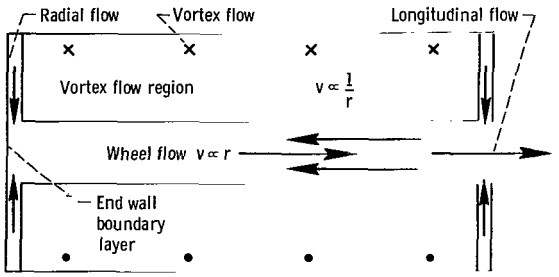

(a) Vortex tube geometry with large length to diameter ratio.

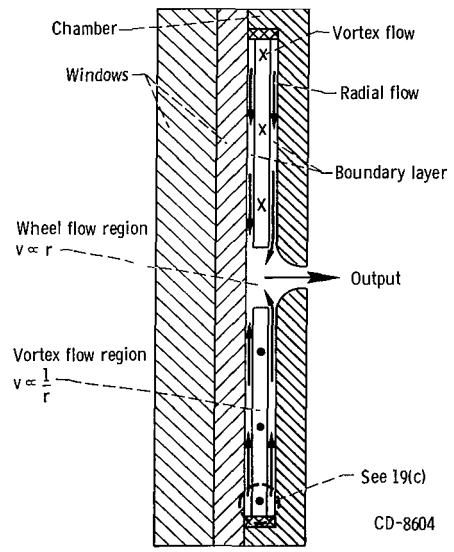

(b) Combustor with vortexing flow.

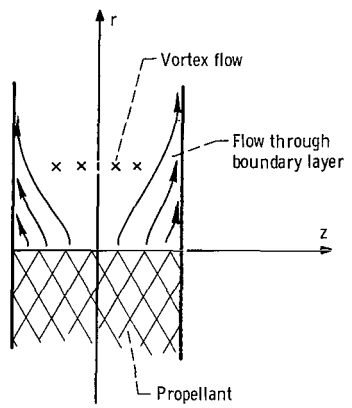

(c) Streamline pattern in vicinity of burning propellant surface.

Figure 19. - Flow fields in vortex geometries.

Flow of the mass added by combustion takes place primarily through the boundary layers on the top and bottom walls of the motor, as shown in figure 19(c) (refs. 11 and 13). The central core region of longitudinal flow corresponds approximately to the nozzle diameter.

Tangential Velocity Calculation

The magnitude of the tangential velocity may be determined by using the measured radial pressure distribution and assuming the presence of a free vortex. The equation of motion for vortex flow is given by

$$\frac{\bar{v}_\theta^2}{R} = \frac{g}{\rho}\frac{\partial P}{\partial R} \tag{6}$$

where the viscous term is neglected (ref. 13). The angular velocity is expressed as the ratio of the circulation to the radius

$$\bar{v}_\theta = \frac{\Gamma}{R}$$

Substituting for v_θ and for ρ, where $P/\rho^\gamma = B$, and integrating yield

$$-\frac{\Gamma^2}{2}\left(\frac{1}{R_2^2} - \frac{1}{R_1^2}\right) = \frac{gB^{1/\gamma}}{\frac{\gamma - 1}{\gamma}}\left[P_2^{(\gamma-1)/\gamma} - P_1^{(\gamma-1)/\gamma}\right] \tag{7}$$

The circulation Γ was evaluated by using the measured pressure distribution. The tangential velocity was then calculated at a given radius

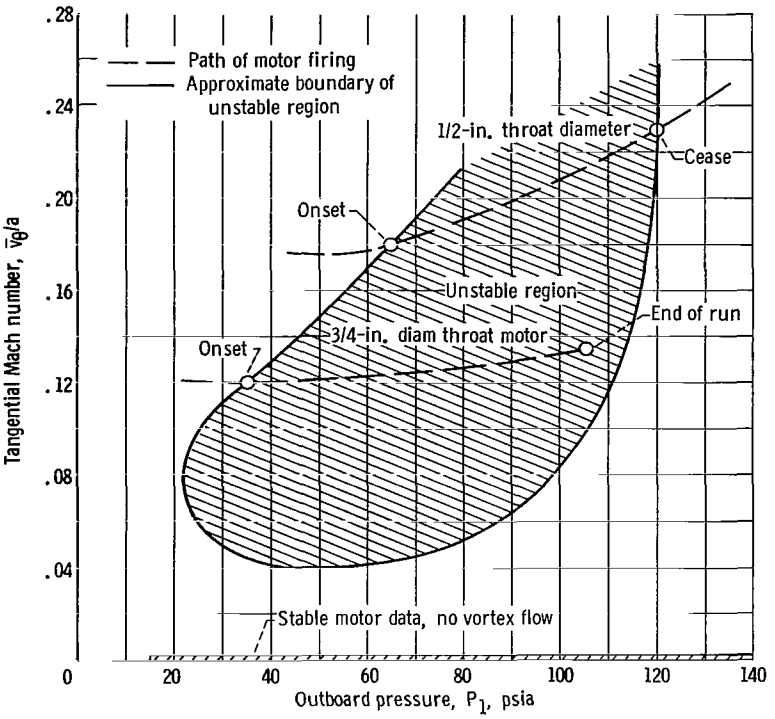

Figure 20. - Approximate region of unstable combustion.

using the ratio of the circulation to the radial distance. The results of these calculations are shown in figure 20 where the tangential Mach number at the outboard position is plotted as a function of the chamber pressure for the onset and cessation points. Average values of the chamber pressure from figure 3 for both the onset and cessation of the oscillations were used. The change in Mach number during the unsteady portion of the motor firings is represented by the dashed lines within the stability boundaries. These limited data were used to construct a region of unstable motor operation for the burner geometries used in this study. The unstable region was bounded at low tangential Mach numbers, since a series of motor firings, made without tangential gas injection and covering the plotted pressure range, showed no incidence of instability. This implies that the system losses (primarily the convective nozzle flow) in the absence of tangential flow exceeded the propellant driving due to pressure coupling only. In addition, the diameter of the motor at which the vortex flow within the motor reaches sonic velocity was calculated by using equation (7) and the measured pressure distribution. The results are given in table II. Because the central region of the vortex is composed of gas flow in the longitudinal direction, the calculated choke points for the 3/4-inch motor are hypothetical. The position of the choke condition must exist at or near the throat. However, for the 1/2-inch motor the calculated choke diameter is significantly larger than the real throat. Therefore, the location of choked flow exists within the combustor. Since the

TABLE II. - CALCULATED THROAT DIAMETERS

BASED ON FREE VORTEX FLOW

Chamber throat diameter, in.	Chamber pressure behavior	Choked diameter, in.	Chamber pressure, psia
1/2	Onset of instability	0.98	65
	Cessation of instability	1.24	120
3/4	Onset of instability	0.62	35
	Run end	.78	105

flow area increases in the vicinity of the nozzle, the possibility of supersonic flow within the motor exists. Subsequent expansion of the flow to atmospheric pressure would be accompanied by the presence of shock waves. The influence of shock formation on stability and on the pitting in the top window are uncertain. In addition, table II shows that the effective throat area is smaller at the onset of instability than at the cessation condition.

Analysis of Data

The pattern of motor behavior, relative to instability, is not well delineated by the foregoing results. Use of a different propellant, motor geometry, or run sequence might change the results substantially. It is necessary, therefore, to consider the test results in light of analytical developments in order to determine if a predictable pattern of instability occurred. Recently, calculations based on a nonlinear theory (ref. 14) have been carried out for a motor with a hollow cylindrical grain (ref. 15). These calculations have also been extended to the case in which tangential flows existed in the motor (refs. 16 and 17). A low, steady tangential velocity can readily excite the traveling transverse mode of combustion instability. This sensitivity to tangential flows has been examined in recent studies (refs. 18 and 19) and a quasi-steady velocity-dependent combustion mechanism was developed. Although the nonlinear results of references 15 and 17 show the correct qualitative trend for explaining the experimental data, it is necessary to specify numerous undetermined variables. The simpler analytical approach of reference 18, therefore, was used for comparison with the data herein, thereby adhering to the principle of Occams Razor. In reference 18 the energy release from the combustion was assumed to be dependent on the absolute value of the relative velocity. For the case of a traveling transverse wave existing in the cavity with no mean throughflow, the addition of energy is identical during the high-pressure and low-pressure portions of the cycle, if the density effect is neglected, as shown in figure 21 (taken from ref. 18). Figure 21(a) shows the pressure oscillation, and 21(b) shows the corresponding velocity and energy release curves. Hence, in accordance with the Rayleigh criterion, the system is in a condition of neutral stability. Superposition of a mean tangential flow on the oscillating velocity causes an increase in the energy release during the high-pressure part of the cycle at the expense of the low-pressure portion, as shown in figure 21(c). Therefore, wave driving can be achieved by biasing the flow in the direction of wave motion. No time delay was

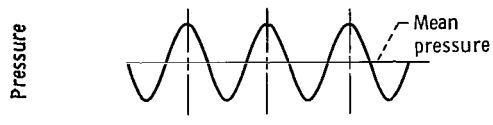

(a) Pressure oscillation.

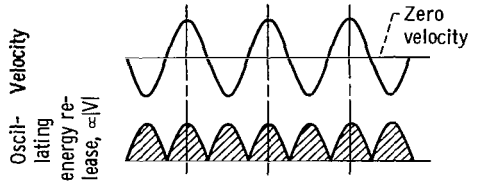

(b) Velocity oscillation for traveling wave with no steady flow in plane of wave.

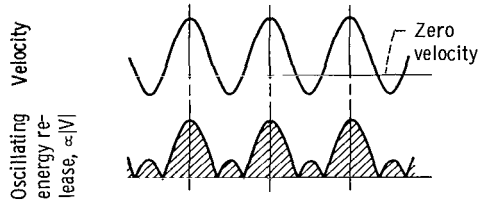

(c) Velocity oscillation for traveling wave with steady flow in direction of wave.

Figure 21. - Phase relations of spinning transverse waves (ref. 18).

assumed between the combustion perturbation and the propellant response.

The burning rate of the propellant used in this study was assumed to behave in a quasi-steady fashion, in accordance with the following expression:

$$r = CP^n + k(\rho v)^m \tag{8}$$

The rate of energy release was assumed to be directly proportional to the burning rate, $w \propto r$. Manipulation of the burning rate expression yields

$$\frac{w}{C\bar{P}^n} = \left(\frac{P}{\bar{P}}\right)^n + \frac{k(\bar{\rho}a)^m}{C\bar{P}^n}\left(\frac{\rho v_\theta}{\bar{\rho}a}\right) \tag{9}$$

where the bar represents average values during oscillatory burning. Maslen and Moore (ref. 3) have given the inviscid solutions for the pressure and density ratios for the first traveling transverse mode. Evaluated at the chamber wall the solutions are

$$\frac{P}{\bar{P}} = 1 - 0.698\,\epsilon\,\cos t \tag{10}$$

$$\frac{\rho}{\bar{\rho}} = 1 - 0.582\,\epsilon\,\cos t \tag{11}$$

$$\frac{v_\theta}{a} = \frac{\bar{v}_\theta}{a} + 0.316\,\epsilon\,\cos t \tag{12}$$

where equation (12) has been modified to include a steady-state component $\bar{v}_\theta/a$. Substitution of these quantities into equation (9) yields

$$\frac{w}{C\bar{P}^n} = (1 - 0.698\,\epsilon\,\cos t)^n + C_1(1 - 0.582\,\epsilon\,\cos t)^m\left(\left|\frac{\bar{v}_\theta}{a} + 0.316\,\epsilon\,\cos t\right|\right)^m \tag{13a}$$

Hence, by assigning values for the amplitude factor ϵ, the pressure exponent n, the parameter

$$C_1 = \frac{k(\bar{\rho}a)^m}{C\bar{P}^n} \tag{13b}$$

the erosive exponent m, and the tangential Mach number, the expression may be evaluated for $w/C\bar{P}^n$, which is assumed proportional to the instantaneous energy release.

The oscillating component of the energy release in phase with the pressure (ref. 18) is given by

$$\tilde{w} = \int_{-\pi/2}^{\pi/2} (w - \bar{w})dt + \int_{\pi/2}^{3\pi/2} (\bar{w} - w)dt \tag{14}$$

where $\bar{w}$, the average energy release during oscillation, is

$$\bar{w} = \frac{1}{2\pi} \int_0^{2\pi} w \, dt \tag{15}$$

The ratio of the oscillating energy exchange to the average energy $\tilde{w}/\bar{w}$ over a cycle was calculated for tangential Mach numbers $\bar{v}_\theta/a$ from 0 to 0.25 and an axial Mach number of zero. These flow conditions correspond to the region adjacent to the burning propellant in the motor geometry used in this study. The response N of the energy release to a pressure perturbation, defined as

$$N \equiv \frac{\tilde{w}/\bar{w}}{\tilde{P}/\bar{P}} \tag{16}$$

was obtained as a function of tangential Mach number for various values of C_1. The calculated response curves for peak-to-peak amplitudes of 7 and 49 percent are shown in figures 22 and 23, respectively. These values were chosen as representative of the noise level in the motors at the onset of instability and of the equilibrium amplitude of the oscillation. The pressure exponent n was equal to 0.4 and the erosive exponent m equal to 0.6. The pressure exponent was based on the experimental strand data, whereas the erosive exponent was chosen to yield agreement between the data and the calculations. These response curves show that driving the transverse traveling wave could occur over a broad range of biasing tangential Mach number $\bar{v}_\theta/a$. This range is limited by estab-

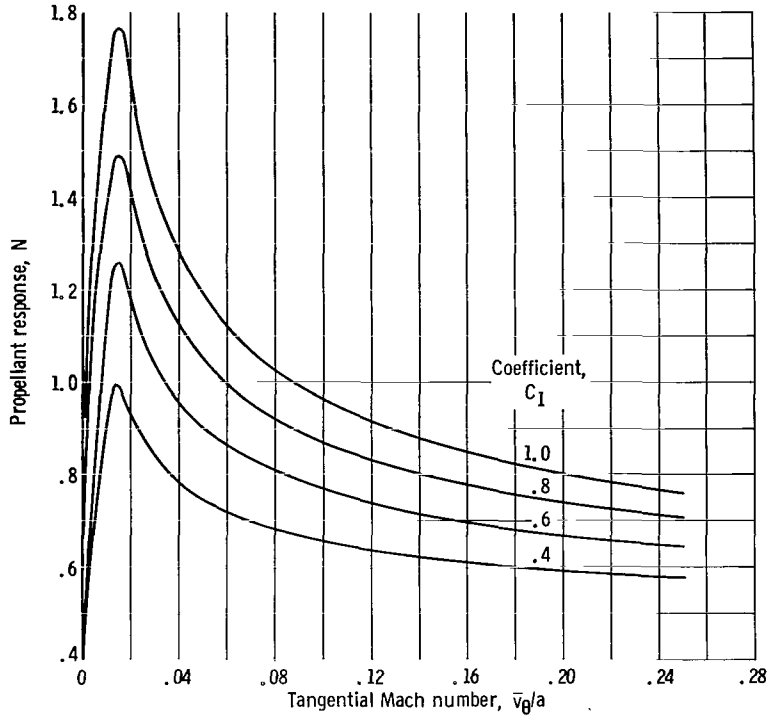

Figure 22. - Calculated response variation with Mach number. Peak-to-peak pressure amplitude, 7 percent.

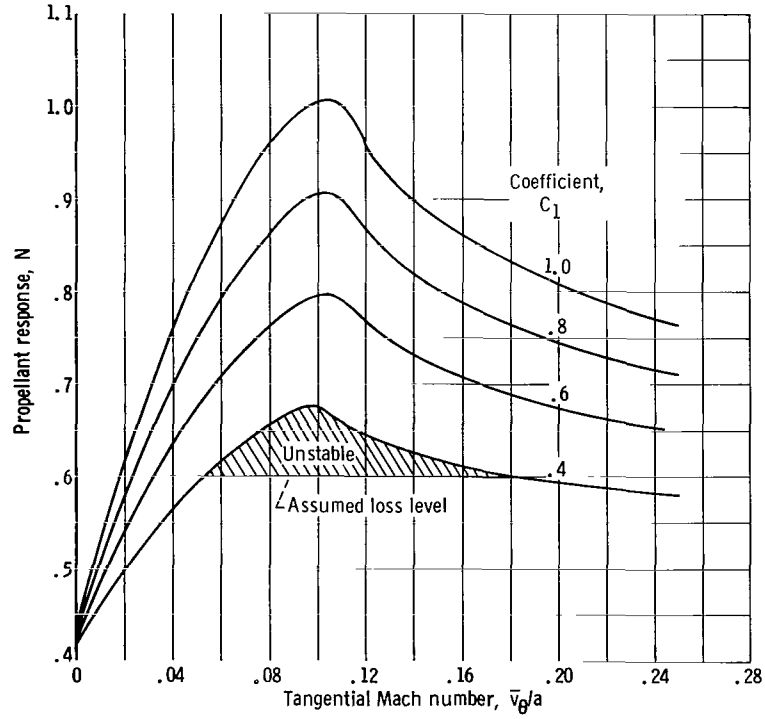

Figure 23. - Calculated response variation with Mach number. Peak-to-peak pressure amplitude, 49 percent.

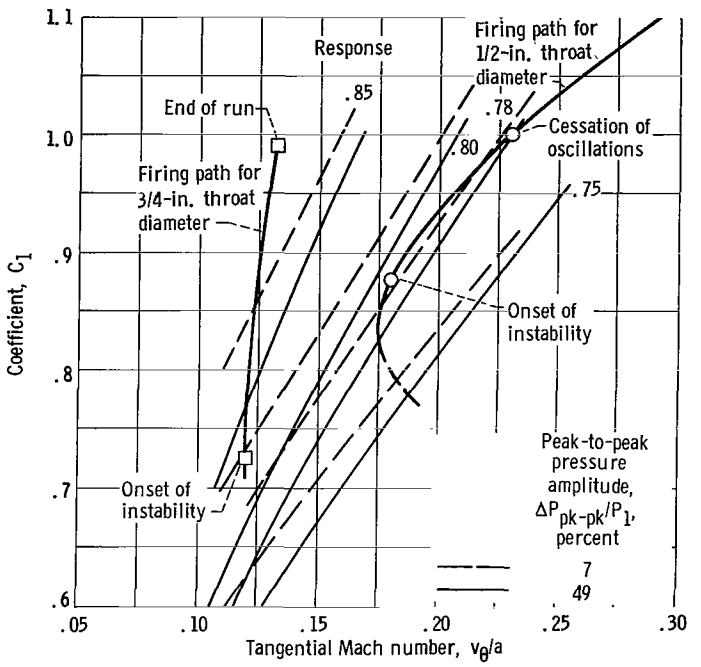

Figure 24. - Comparison of experimental motor data with calculated response curves.

lishing a value for the losses in a system due to various components, that is, nozzle, propellant, baffles, and head cavity. As an example (fig. 23), these combined losses were assumed to be equal to 0.6 for the case where C_1 is equal to 0.4. Hence, for a motor having a response N greater than 0.6 and C_1 equal to 0.4, driving would occur over the tangential Mach number range from 0.05 to 0.18. It is noted that the velocity sensitivity of the propellant exerted a predominant influence on the shape of the response curve, whereas the pressure sensitivity altered the magnitude of the response by a constant amount.

Crossplotting the data from figures 22 and 23 gives the two families of curves with amplitudes of 7 and 49 percent (fig. 24). In order to evaluate the parameter C_1 as a function of pressure, k was determined by using the erosive burning rate of 0.02 from reference 20 and a $\bar{v}_\theta$ of 600 feet per second with a density of 0.1 pound per cubic foot. The values used for evaluating C_1 were

$$\bar{\rho} = 0.1 \text{ lb/ft}^3 \text{ at 60 psia}$$

$$C = 0.016 \text{ in.}^3/(\text{lb})(\text{sec})$$

$$a = 5000 \text{ ft/sec}$$

$$k = 0.001725 \text{ (in.)}(\text{ft}^2)/\text{lb}$$

$$n = 0.4$$

$$m = 0.6$$

The representative paths traced by the motor firings are shown in figure 24. For the 1/2-inch-diameter throat motor, as the motor operating condition crosses the 7-percent

amplitude curve (the assumed noise level in the combustor) with a response factor of 0.78, the motor goes unstable. Instability continues until the motor firing path recrosses the 0.78 response curve, which occurs at an amplitude corresponding to that which existed in the unstable motor (~50 percent). Continued burning of the motor results in stable operation because the response curve is not crossed again. The tangential Mach numbers $\bar{v}_\theta/a$ at the onset and cessation points of instability match the experimental values shown in figure 20 (p. 25) when an erosive exponent of 0.6 is used. The starting point of the 1/2-inch motor is at a low C_1 value and high tangential flow, since the initial flow from the gas generator establishes tangential flow prior to the ignition of the main propellant. This tangential flow is not initially subjected to the radial momentum of the combustion gases from the main charge. After ignition of the main propellant charge, the tangential velocity decreased. This sequence of events occurred at relatively low chamber pressures (<40 psia). With increasing pressure, the tangential Mach number increased steadily. The low pressure levels encountered at the test start exclude accurate calculations of $\bar{v}_\theta/a$. The initial crossing of the response curves at low $\bar{v}_\theta/a$ values presumably occurred prior to complete ignition of the main charge.

Similarly, the 3/4-inch-diameter throat motor followed the firing path shown in figure 24. As the motor firing condition reached a value of N of approximately 0.8, with an amplitude of 7 percent, instability began and continued throughout the remainder of the firing. The slightly higher response value for the 3/4-inch-diameter throat motor might be indicative of a larger nozzle loss relative to the 1/2-inch diameter throat motor. The tangential Mach number at the onset of instability matches the experimental value of 0.12 given in figure 20.

Elimination of Instability

The experimental configuration, incorporating the use of radially drilled rings (fig. 6, p. 15), proved effective in preventing the occurrence of instability. Figure 7 (p. 16) shows that the chamber pressure reached and exceeded the onset pressure for instability with no ring in the motor, although this occurred at a later time during the motor firing. The path of the motor firing, therefore, was such that it never crossed the threshold-response curve as in the no-ring case. For example, in the motor with a 1/2-inch-diameter throat, if $\bar{v}_\theta/a$ is assumed to be equal to the no-ring test at a corresponding time during the test, C_1 has a value of 0.7 and 0.88 at $\bar{v}_\theta/a$ equal to 0.18 and 0.23, respectively. The motor firing path never crossed the 0.78 response-factor line and, hence, operated stably. Regardless of the three ring positions, the nozzle-flow blockage effect of the swirling flow was eliminated, which prevented the chamber pressure from rising to values obtained with the unbaffled motors.

Figure 8 (p. 17) shows similar results for the 3/4-inch-diameter throat motor where the maximum chamber pressure reached only 50 pounds per square inch absolute. Use of the ring again prevented the excessive pressure rise due to the nozzle blockage effect, and the path of motor operation remained below the required response curve for instability (with the system losses exceeding the gains).

SUMMARY OF RESULTS

Transverse mode combustion instability was initiated in a two-dimensional circular combustor that utilized a progressively burning gas generator to feed hot gas tangentially into the main chamber through a small jet. The effect of oxidizer particle size on the amplitude of the pressure oscillations was determined for two different initial port-to-throat diameter ratios. The onset and cessation points of instability were characterized by the tangential Mach number and chamber pressure. The tangential flow caused the pressure to rise 2 to 3 times greater than expected as a result of added mass from the generator and erosive burning. It was concluded that the swirling flow gave rise to a strong vortex, with an attendant pressure distribution, which caused a nozzle blockage effect. Elimination of the vortex in the region of the nozzle by use of radially drilled rings prevented the excessive pressure rise as well as eliminating the occurrence of instability.

Calculations of the propellant response, based on a wave amplification mechanism due to preferential energy additon with flow biasing, offered an explanation of the experimental data. The rate of energy addition was assumed proportional to the propellant burning rate which was sensitive to both pressure and velocity.

CONCLUDING REMARKS

The calculated response factors presented herein are dependent on both the velocity and pressure sensitivity of the propellant burning process. Because of the wave amplification mechanism assumed, the velocity sensitivity exerted the predominant influence on the appearance and disappearance of instability (i. e., the shape of the response curves), whereas pressure changed the magnitude of the response by a constant amount independent of velocity. Accordingly, it is the propellant erosion that introduced the velocity sensitive term. Hence, a small amount of erosion was sufficient to exert a profound influence on the stability behavior. Similar results have been observed in the nonlinear calculations of reference 15 in which a small amount of erosion exerted a drastic change in stability boundaries.

The initial ratios (port area/throat area) for the motors used in this study were 100 and 45 for the 1/2- and 3/4-inch-diameter throat motors, respectively. Both these ratios are high in comparison with operating rocket motors. Hence, the extrapolation of these data to real systems for a given tangential velocity at the propellant surface would yield less severe swirling at the nozzle entrance. The fractional rise in chamber pressure, therefore, would not be as large as that obtained in the present study. However, instability may result if the combined pressure and velocity sensitivity are such that the propellant response exceeds the system losses.

Lewis Research Center,
National Aeronautics and Space Administration,
Cleveland, Ohio, July 15, 1966,
128-31-06-03-22.

REFERENCES

1. Mayhue, Robert J.: NASA Scout ST-1 Flight-Test Results and Analyses, Launch Operations, and Test Vehicle Description. NASA TN D-1240, 1962.

2. Flandro, G. A.: Roll Torque and Normal Force Generation in Acoustically Unstable Rocket Motors. AIAA J., vol. 2, no. 7, July 1964, pp. 1303-1306.

3. Maslen, Stephen H.; and Moore, Franklin K.: On Strong Transverse Waves Without Shocks in a Circular Cylinder. J. Aeron. Sci., vol. 23, no. 6, June 1956, pp. 583-593.

4. Swithenbank, J.; and Sotter, G.: Vortex Generation in Solid Propellant Rockets. AIAA J., vol. 2, no. 7, July 1964, pp. 1297-1302.

5. Heidmann, Marcus F.: Oxygen-Jet Behavior During Combustion Instability in a Two-Dimensional Combustor. NASA TN D-2725, 1965.

6. Price, E. W.: Experimental Solid Rocket Combustion Instability. Tenth Symposium (International) on Combustion. Combustion Institute, 1965, pp. 1067-1080.

7. Povinelli, Louis A.; and Heidmann, Marcus F.: Study of Transverse Mode Solid-Propellant Combustion Instability. Proceedings of the First ICRPG Combustion Instability Conference, CPIA Pub. no. 68, Jan. 1965, pp. 409-411.

8. Povinelli, Louis A.: Effect of Oxidizer Particle Size on Additive Agglomeration. NASA TN D-1438, 1962.

9. Mager, Artur: Approximate Solution of Isentropic Swirling Flow Through a Nozzle. ARS J., vol. 31, no. 8, Aug. 1961, pp. 1140-1148.

10. Morrell, Gerald; and Pinns, Murray L.: Effect of Oxidizer Particle Size on Solid-Propellant Combustion Stability. NASA TN D-2736, 1965.

11. Rosenzweig, M. L.; Ross, D. H.; and Lewellen, W. S.: On Secondary Flows in Jet-Driven Vortex Tubes. J. Aerospace Sci., vol. 29, no. 9, Sept. 1962, pp. 1142-1143.

12. Swithenbank, J.: Non-Linear Behavior of Solid Propellant Rocket Combustion Instability. Proceedings of Second ICRPG Combustion Conf., CPIA Pub. no. 105, vol. 1, May 1966, pp. 719-760.

13. Savino, Joseph M.; and Keshock, Edward G.: Experimental Profiles of Velocity Components and Radial Pressure Distributions in a Vortex Contained in a Short Cylindrical Chamber. NASA TN D-3072, 1965.

14. Priem, Richard J.; and Guentert, Donald C.: Combustion Instability Limits Determined by a Nonlinear Theory and a One-Dimensional Model. NASA TN D-1409, 1962.

15. Povinelli, Louis A.: One-Dimensional Nonlinear Model for Determining Combustion Instability in Solid Propellant Rocket Motors. NASA TN D-3410, 1966.

16. Priem, Richard J.: Influence of Combustion Process on Stability. NASA TN D-2957, 1965.

17. Povinelli, Louis A.: Nonlinear Combustion Stability Limits for Solid-Propellant Motors Including Vortex Flow Effects. Proc. of Second ICRPG Combustion Conf. CPIA Pub. no. 105, vol. 1, May 1966, pp. 761-767.

18. Heidmann, M. F.; and Feiler, C. E.: Evaluation of Tangential Velocity Effects on Spinning Transverse Combustion Instability. NASA TN D-3406, 1966.

19. Heidmann, Marcus F.: Oscillatory Combustion of a Liquid-Oxygen Jet with Gaseous Hydrogen. NASA TN D-2753, 1965.

20. Marklund, Tage; and Lake, Arne: Experimental Investigation of Propellant Erosion. ARS J., vol. 30, no. 2, Feb. 1960, pp. 173-178.

"The aeronautical and space activities of the United States shall be conducted so as to contribute . . . to the expansion of human knowledge of phenomena in the atmosphere and space. The Administration shall provide for the widest practicable and appropriate dissemination of information concerning its activities and the results thereof."

—NATIONAL AERONAUTICS AND SPACE ACT OF 1958

NASA SCIENTIFIC AND TECHNICAL PUBLICATIONS

TECHNICAL REPORTS: Scientific and technical information considered important, complete, and a lasting contribution to existing knowledge.

TECHNICAL NOTES: Information less broad in scope but nevertheless of importance as a contribution to existing knowledge.

TECHNICAL MEMORANDUMS: Information receiving limited distribution because of preliminary data, security classification, or other reasons.

CONTRACTOR REPORTS: Technical information generated in connection with a NASA contract or grant and released under NASA auspices.

TECHNICAL TRANSLATIONS: Information published in a foreign language considered to merit NASA distribution in English.

TECHNICAL REPRINTS: Information derived from NASA activities and initially published in the form of journal articles.

SPECIAL PUBLICATIONS: Information derived from or of value to NASA activities but not necessarily reporting the results of individual NASA-programmed scientific efforts. Publications include conference proceedings, monographs, data compilations, handbooks, sourcebooks, and special bibliographies.

Details on the availability of these publications may be obtained from:

SCIENTIFIC AND TECHNICAL INFORMATION DIVISION

NATIONAL AERONAUTICS AND SPACE ADMINISTRATION

Washington, D.C. 20546